WEDGE-AND-STRIP ANODES FOR CENTROID-FINDING POSITION-SENSITIVE PHOTON AND PARTICLE DETECTORS

C. Martin, P. Jelinsky, M. Lampton, R. F. Malina

Space Sciences Laboratory
University of California
Berkeley, California 94720

and

H. O. Anger

Donner Laboratory
Lawrence Berkeley Laboratory
University of California
Berkeley, California 94720

Revised: Feb. 9, 1981

This work was supported by Cal Space grant CS 37-79,
NASA contracts NAS-5-24445 and NAS-8-32577 and the
U.S. Department of Energy under Contract W-7405-ENG-48.

ABSTRACT

We discuss new anode geometries, employing position dependent charge partitioning, which can be used with microchannel plates, planar proportional counters, and mesh dynode electron multipliers to obtain a two-dimensional position signal from each detected photon or particle. Only three or four anode electrodes and signal paths are required, yet images comprised of a number of detected events have little geometric distortion and the resolution is not limited by thermal noise inherent in resistive sheet anodes. We present an analysis of the geometrical image nonlinearity in the relationship between event centroid location and the charge partition ratios. Fabrication and testing of two wedge-and-strip anode systems are discussed. Images obtained with EUV radiation and microchannel plates that verify the predicted performance of this readout system are shown. We emphasize that the spatial resolution of the wedge-and-strip anode is in no way limited by the coarseness of the anode conductor pattern. The resolution is of the order of 0.4% of the image field size, and could be further improved by adopting low noise signal circuitry. Tradeoffs encountered in the design of practical X-ray, EUV and charge particle image systems are discussed.

INTRODUCTION

In many laboratory and spaceborne applications involving the detection of photons or charged particles, position-sensitive detectors have become increasingly important because they allow spatial information to be recovered efficiently. In general, a position-sensitive detector consists of a photocathode, a charge multiplication element which preserves positional information, a coordinate encoding charge collection anode, and coordinate decoding electronics. An example, which incorporates microchannel plates (MCP) as the charge multiplication device, is illustrated in Fig. 1. The key element is the electrode, usually the anode, which divides the detector's output charge among several output terminals with relative amplitudes which depend upon the event's position. Signal processing electronics connected to these outputs can recover the event position in essentially real time, allowing an image to be accumulated whose signal-to-noise ratio is ultimately limited only by Poisson statistics.

Anodes for position sensing are of two kinds: (1) discrete anode elements intended to identify each event position digitally with a resolution limited to the spatial size of the anode elements, and (2) electrode geometries that give a continuous variation in output from which event positions can be recovered by analog means. If a separate signal amplifier, discriminator, and scaler is provided for each pixel in a discrete-anode system, the high counting rate advantages of a fully parallel system are realized, but the equipment is quite complex if high resolution images are needed. For this reason, most discrete anodes use some sort of coincidence arrangement to minimize the number of associated electronics channels, at the expense of high count rate performance.

Figure 1: Schematic representation of a position sensitive detector comprising a cascaded pair of microchannel plates, an anode, and signal processing electronics. The position sensitivity is due to the anode, which delivers signals having relative amplitudes that depend on position.

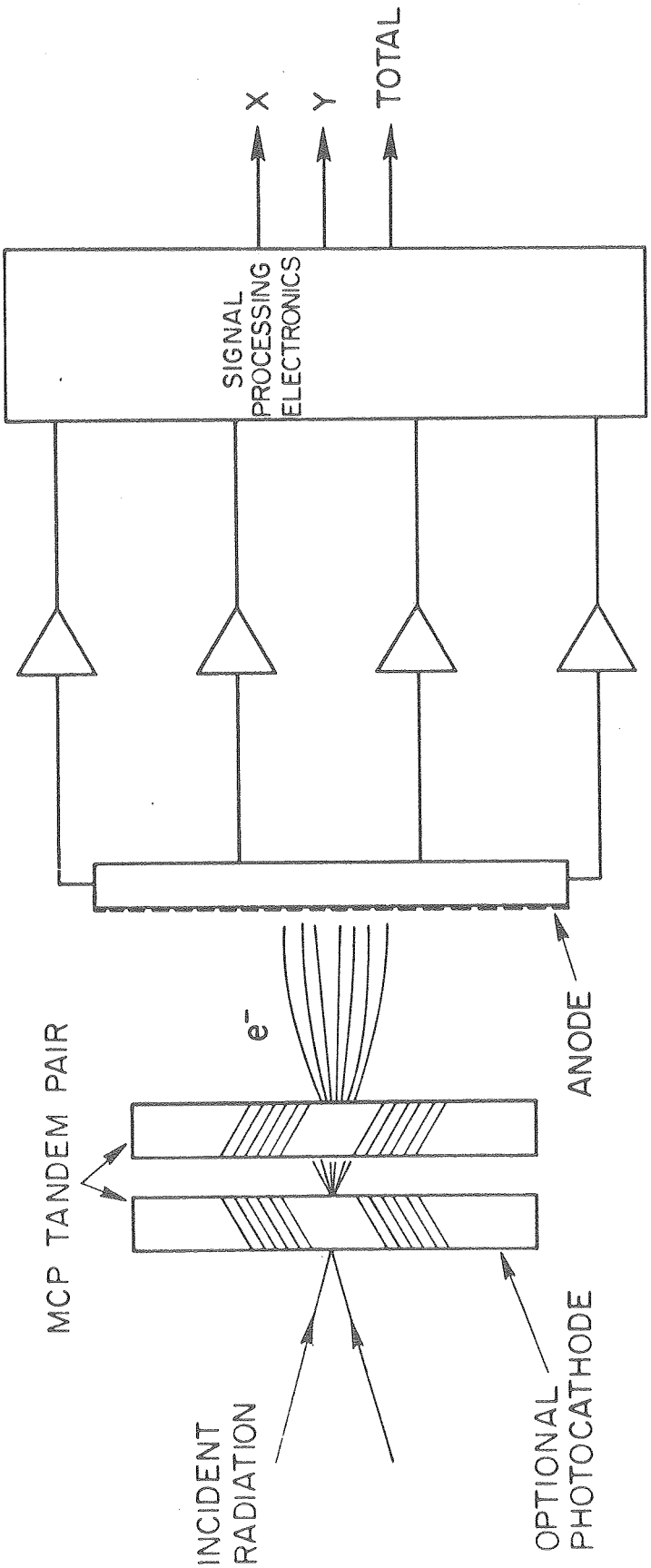
X
Y
TOTAL
SIGNAL PROCESSING ELECTRONICS
e⁻
ANODE
MCP TANDEM PAIR
INCIDENT RADIATION
OPTIONAL PHOTOCATHODE

Figure 1

In contrast, analog coordinate readout anodes can typically achieve a spatial resolution ten to one thousand times finer than the spatial structure of the anode, since the accuracy with which the ratio of two charge signals may be computed is a very small fraction of the total charge. The analog ratio technique measures the centroid of the charge cloud liberated by the multiplication element and thereby recovers the position of a single primary event or alternatively the centroid position of simultaneous multiple primary events. Digitized position coordinates, usually essential for data transfer, telemetry, and storage, are then obtained from an analog to digital converter. Thus in terms of performance, anode simplicity, and electronics requirements, the analog position sensing anode is often the better alternative.

Analog-encoding anodes are of two varieties: (1) the resistive anode[1], employed with solid state detectors, gas counters, and microchannel plates, and (2) the discrete conductor segmented anodes such as the one dimensional jeu de jacquets (backgammon) anode[2], the one dimensional graded density cathode[3], and the two dimensional quadrant anode[4,5], in which the position dependence of the relative amounts of charge arriving at several electrodes is utilized. Although the resistive anode has been well studied and has geometries which can make it theoretically distortionless[6], it is subject to an irreducible thermal charge noise which limits its spatial resolution. The segmented anode does not share this limitation; its noise level is determined by partition noise and by the associated charge amplifier noise. With present technology, the amplifier noise can easily be kept to below 10^3 electrons rms. We shall show that with signal charges of 10^6 - 10^7 electrons, 10^6 - 10^7 pixel images should in principle be obtainable.

The simple quadrant anode is indeed capable of very high spatial resolution and as a further bonus can accomodate very high counting rates by avoiding the introduction of charge diffusion inherent in resistive anodes into the signal processing. Its drawback is that its mapping of spatial coordinates into charge ratios is highly distorted, with a high magnification in the center of the field of view and diminishing magnification elsewhere. The wedge-and-strip anode described in the next section overcomes this geometric distortion problem.

I. ANGER'S WEDGE-AND-STRIP ANODE

An alternative anode was proposed some time ago by H. O. Anger[7] which exhibits the desirable features of the quadrant anode yet which can cover a rectangular field of view with essentially distortionless encoding of xy positions into charge ratios. The four electrodes in Anger's design have the form of a repetitive pattern of wedges and strips as shown in Figure 2. The wedges are all identical, and furnish a charge collecting area which varies linearly with the y-coordinate of the charge centroid position. Consequently the y coordinate of each event centroid may be obtained from the ratio (A-B)/(A+B) or A/(A+B), where A and B are the electrical charge signals collected by the two wedge groups. Between the wedge pairs are pairs of stips, whose individual widths vary linearly in the x direction. The width of one set of stips increases in the x direction while the width of the other set decreases in the same direction. Consequently, the x coordinate of each event centroid may be obtained from the ratio (C-D)/(C+D) or C/(C+D), where C and D are charge signals collected by the two strip groups, assuming that the charge footprint is large enough as detailed below.

In the center of the anode, the area fractions occupied by each of the four conductors is 25%. Away from the center, the relative areas occupied

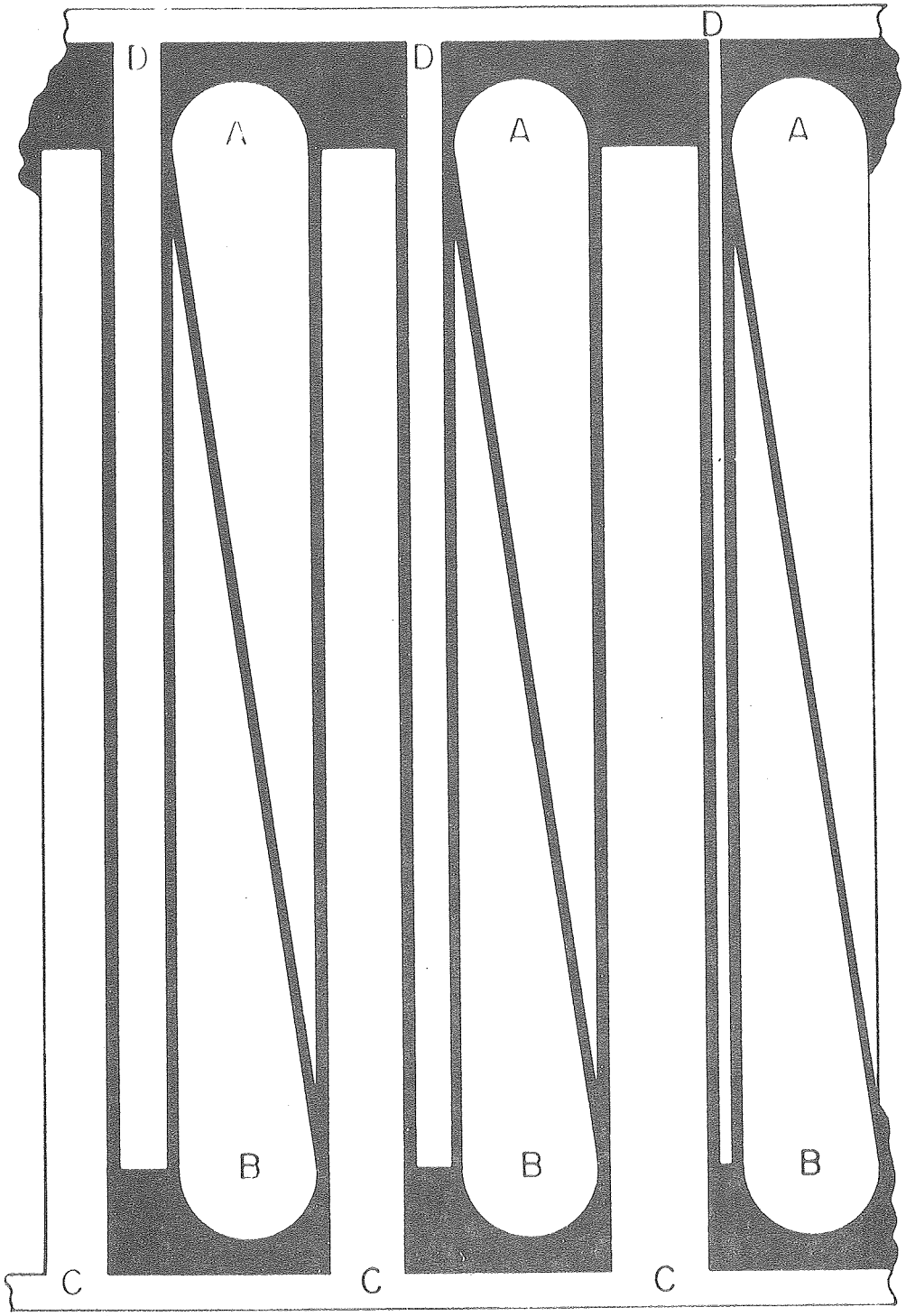

$$X = \frac{C}{C + D}$$

$$Y = \frac{A}{A + B}$$

Figure 2

Figure 2: A portion of a four-electrode anode pattern devised by H.O. Anger (1966). Black regions are insulators, and white areas are conductors. All wedges marked "A" are connected together by a common conductor located beneath the anode plane; similarly the "B" wedges are connected to a second common conductor. The ratio of these two signals depends on the y coordinate of the event. Simultaneously, the pairs of strips "C" and "D" are used to determine the x coordinate of the event since the relative widths of these strips vary linearly with x. The coding is nearly distortionless if the size of the deposited charge footprint is somewhat larger than the distance between quartets. The formulae shown are coordinate recovery algorithms appropriate for this geometry.

by the conductors vary linearly with position. It is this property which makes the anode centroid-sensitive, because arriving charge is divided among the electrodes with partition coefficients that are position dependent.

II. DISTORTION

It is clear that if the partition coefficients are to be linear, the footprint of charge arriving at the anode must be large enough to span at least a few of the individual wedges and strips. If the charge were too finely focussed on the anode, large errors would be introduced in the derived x and y position, having a periodicity in x equal to the length of the quartet period of the anode. Denoting this length by p, and modelling the charge density distribution by a Gaussian function with rms radius r, we can express the four electrode signal charges Q_i (normalized to the total detector output charge Q) by the series:

$$\frac{Q_i}{Q} = f_i + 2 \sum_{n=1}^{\infty} \frac{\sin(n\pi f_i)}{n\pi} \exp\left(\frac{-2n^2\pi^2r^2}{p^2}\right) \cos(n\phi_i) \quad i=1,4.$$

In this expression, f_i represents the local fraction of anode area occupied by electrode i, determined at the charge centroid position. In a lossless anode, $f_1 + f_2 = 0.5$ and $f_3 + f_4 = 0.5$ everywhere. The distances d_i separating the charge centroid from the centers of the four nearest electrode elements are represented here by the electrodes' phases within the quartet period, $\phi_i = 2\pi d_i/p$. The first term in the expression, f_i, is the desired component of the anode signal that leads to a spatially linear or undistorted image. The series terms correspond to geometric distortions at increasing spatial frequencies. Then these theoretical signal charge expressions are substituted into estimators of centroid location, e.g. $(Q_1-Q_2)/(Q_1+Q_2)$. The magnitude of the peak position error (expressed as a fraction of the overall anode length) is dominated by the n=1 term in the series if $p \leq r$, and is

$(2\sqrt{2}/\pi)\ \exp(-2\pi^2 r^2/p^2)$. This theoretical position error is less than 1% for $p = 2r$, and diminishes rapidly for smaller p. We conclude that as long as the anode's spatial quartet period is kept smaller than the radius of the deposited signal charge distribution, geometrical distortions will be set by practical limitation such as manufacturing tolerances rather than by any problems inherent to the readout technique.

We have undertaken a measurement of the MCP charge deposition radius and distribution for a range of post acceleration gap potentials and spacings.[8] Preliminary measurements indicate that with an anode gap of 1 cm and an accelerating potential of 300 volts, the charge distribution is approximately Gaussian, and the rms radius is $\sim$1 mm.

III. RESOLUTION

We turn now to a discussion of the spatial resolution which should be obtainable with the wedge-and-strip anode and algorithm shown in Fig. 2. By resolution we mean the random variations in the position determinations of indiyidual events, as distinct from geometrical distortion which is fixed and in principle removable.

Random position errors originate in several ways. First, the arrival of electrons at the anode segments is a random partition noise process governed by four-way multinomial (Bernoulli) statistics. If the subsequent electronic ratio circuitry handles each axis separately, the partition process splits into two independent binomial processes, each acting on about half the total number of signal electrons. Thus, while the mean charge is $\langle Q_i \rangle = f_i Q$, the variance in Q_i is $f_i(1-2f_i)\ Qq$ where q is the electron charge. From these expressions, the rms charge partition blur expressed as a fraction of the anode's overall length is $2\left[f_i(1-2f_i)q/Q\right]^{1/2}$. This blur goes to zero at each end of the axis being examined. It is maximum in the center, where on each axis it reaches a value $(q/2Q)^{1/2}$. If we define the

number of image pixels N as the reciprocal of the worst case two dimensional position variance, then $N = Q/q$, i.e., the number of electrons in each signal pulse is the partition noise limit to the number of resolved picture elements. A tandem microchannel plate can deliver $10^6 - 10^7$ electrons per incident event, and therefore imposes a partition noise limit of $10^6 - 10^7$ pixels. On the other hand, if we define the pixel length as the FWHM of the position distribution, the number of image pixels is $0.361\ Q/q$.

Microchannel plate image systems have additional causes of blur. The individual microchannels have a spacing on the order of 10-30 μm, implying that channel densities are only $10^5 - 10^6\ cm^{-2}$. If a small field of view is to be accommodated the individual channels can introduce a granularity to the image. If a photocathode is employed and is not actually deposited inside the microchannel entrances, additional blur can be introduced depending upon the photoelectron ballistic-trajectory geometry at the cathode. Unlike partition noise, these contributions are independent of detector gain.

A third source of blur is amplifier noise. Charge-sensitive amplifiers have two kinds of random noise: voltage noise, which combined with the detector capacitance and pulse-shaping filter bandwidth is one contribution, and current noise, which is dependent upon the amplifier's input circuitry and the filter time constants. Typically, the charge-sensitive amplifiers used in spectroscopy with solid state detectors have noise levels of 100-1000 electrons rms when employed with detectors of 10-100pF capacitance and pulse-shaping network time constants in the microsecond range. The effect of this amplifier noise Q_N is to perturb the measurements of the signals and hence the positions and amplitudes of the individual events. Analysis shows that the rms blur on one axis is given by $2(1-4f_i + 8f_i^2)^{1/2}Q_n/Q$, where $0 < f_i < 0.5$ is the electrode area fraction as before. This function has a minimum at the center of the field of view; it is maximum at the ends

of the axis, where it reaches twice its minimum value. Adopting our previous worst case two dimensional definition, the limit to the number of pixels imposed by this blur source is $Q^2/8Q_N^2$. In contrast to the previous cases this limit varies as the square of the MCP gain. With MCP output signals in the range of 10^6 - 10^7 electrons, this limit corresponds to 10^5 - 10^7 pixel images if the amplifier noise level is 10^3 electrons.

A fourth potential blur contribution is introduced in the electronic signal processing necessary to obtain the pulse amplitude ratios. Nine amplitude ratio techniques were reviewed by Lampton and Paresce.[1] Here we restrict our comments to three kinds of ratio system. Analog ratio circuits typically use junction diodes as analog exponential and logarithmic converters: the desired ratio is the exponential of the difference of the logarithms of the inputs. Such systems routinely achieve an accuracy of 0.2% over a 10:1 total charge dynamic range and, with some development, should be able to achieve 0.1%, i.e. up to 10^6 pixel images. Analog ratio systems of this kind require about 1 μsec to settle to the required accuracy. They are nicely suited to real time oscilloscope image displays. A second kind of system is based on digitizing all pulse heights and then evaluating the appropriate ratios with digital arithmetic algorithms. Although such numerical manipulations can be implemented with arbitrarily large precision and dynamic range, it is important that the initial pulse height analysis be conducted with sufficient accuracy, for example 10^4 channels are required for 0.1% accuracy over a 10:1 total charge dynamic range. Because the analog system is presently somewhere faster than a 10^4 channel pulse height analyzer and division algorithm, real-time image systems will probably continue to use analog ratio analyzers for some time. Continuing improvements in high speed analog-to-digital converter technology may alter this situation. A third system combines some of the advantages of the analog and digital

methods: a successive-approximation analog-to-digital converter is used, whose signal input is a stretched replica of the numerator pulse and whose reference input is the stretched denominator pulse.

IV. ALTERNATE ELECTRODE PATTERNS

We have found a number of planar conductor patterns that linearly encode event coordinates as charge ratios. We have illustrated some of these, together with their position algorithms, in Figs. 3-5. In general, three conductors are sufficient to provide measurements of the X and Y coordinates of the charge centroid although 4 or 5 electrodes can be used. The number and arrangement of the conductors, along with the choice of scale and origin, dictate the required position algorithm.

For the anode shown in Fig. 3, the electrodes used to obtain the X-position information are a pair of conductors that zigzag between the wedge electrodes. The electrode elements change in width, one decreasing and the other increasing, as they progress in the X-direction. This arrangement eliminates the need for a pair of subplane interconnecting conductors with their attendant substrate perforations. The anode is completely coplanar, which allows it to be made by a simple electro-chemical photographic etching process. Possible position algorithms are the same as those for the anode of Fig. 2, namely $X = (C-D)/(C+D)$ and $Y = (B-A)/(A+B)$ for $-1 \leq X,Y \leq 1$, or $X=C/(C+D)$ and $Y=B/(A+B)$ for $0 \leq X,Y \leq 1$.

A 3-conductor anode is shown in Fig. 4. It is interesting to note that if electrodes A and C are connected together, this pattern reduces to a repetitive wedge pattern, while if B and C are wired together, a repetitive strip pattern having an orthogonal position sensitivity results. An appropriate algorithm is $X = 2A/(A + B + C)$ and $Y = 2B/(A + B + C)$. The advantages of this anode are that it is simpler than the other anodes, it is coplanar and only three low-noise amplifiers are required.

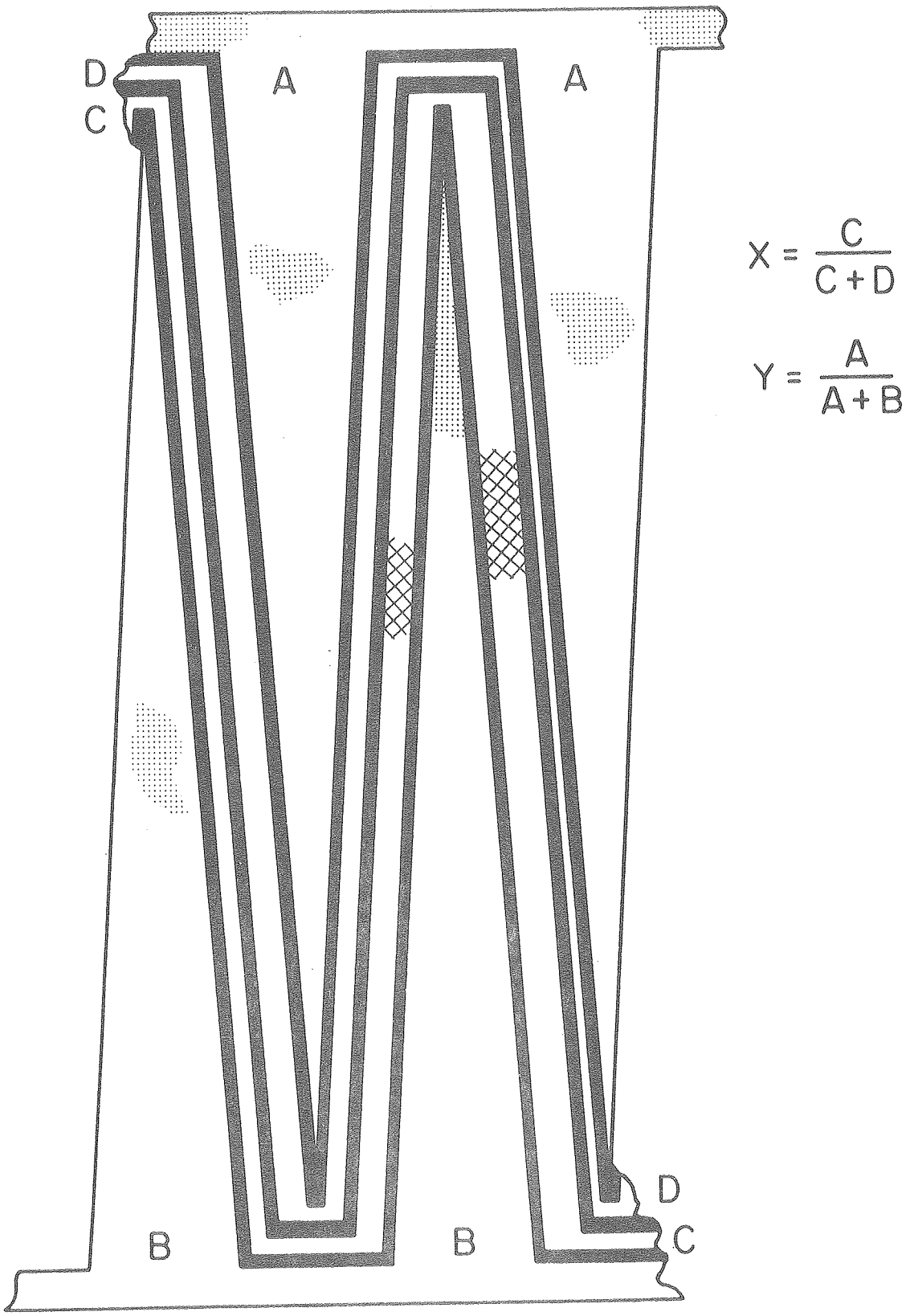

Figure 3: A portion of a four-electrode pattern similar to that of Figure 1 but which requires no penetration of the anode substrate.

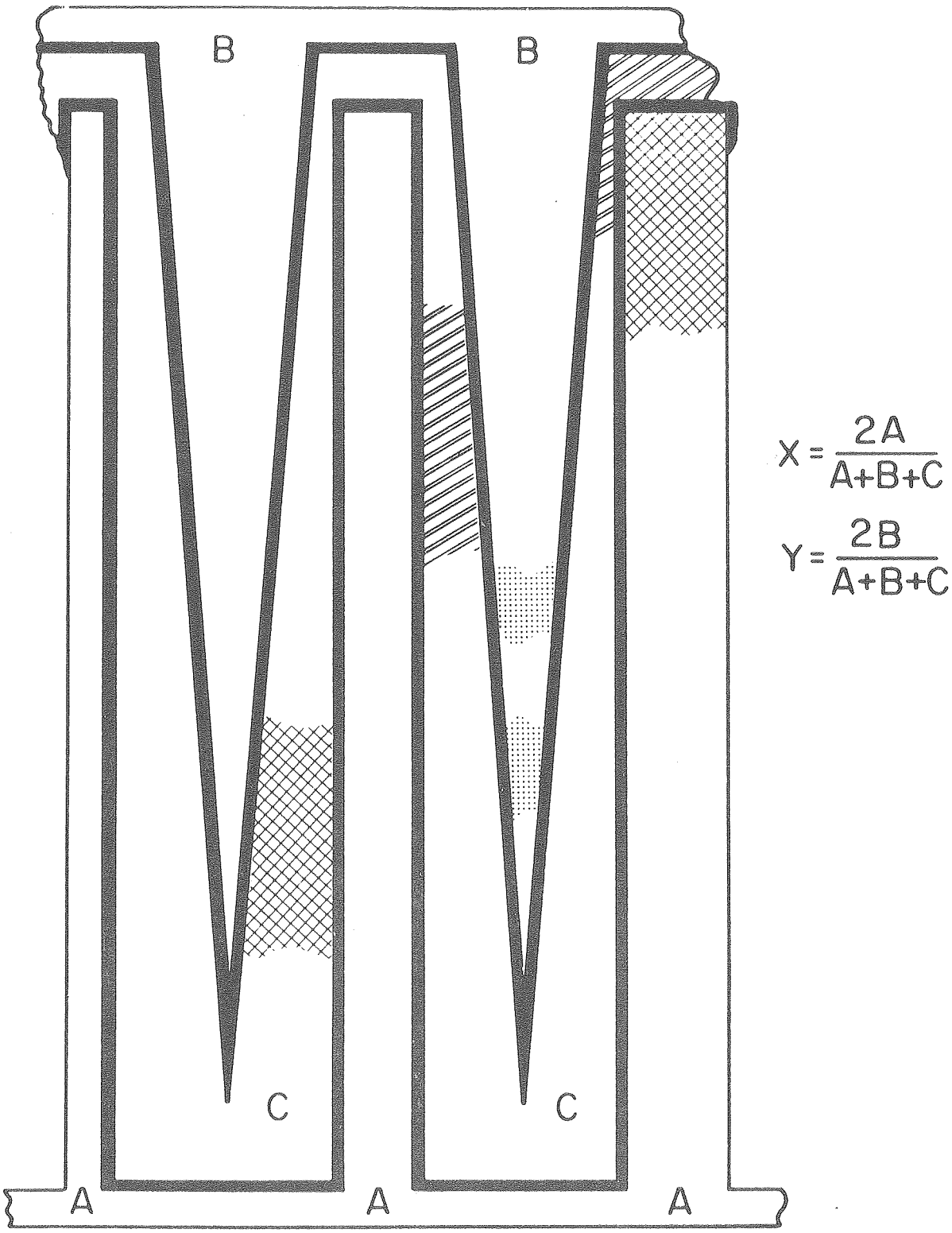

Figure 4: A three-electrode pattern which requires no subplane interconnections.

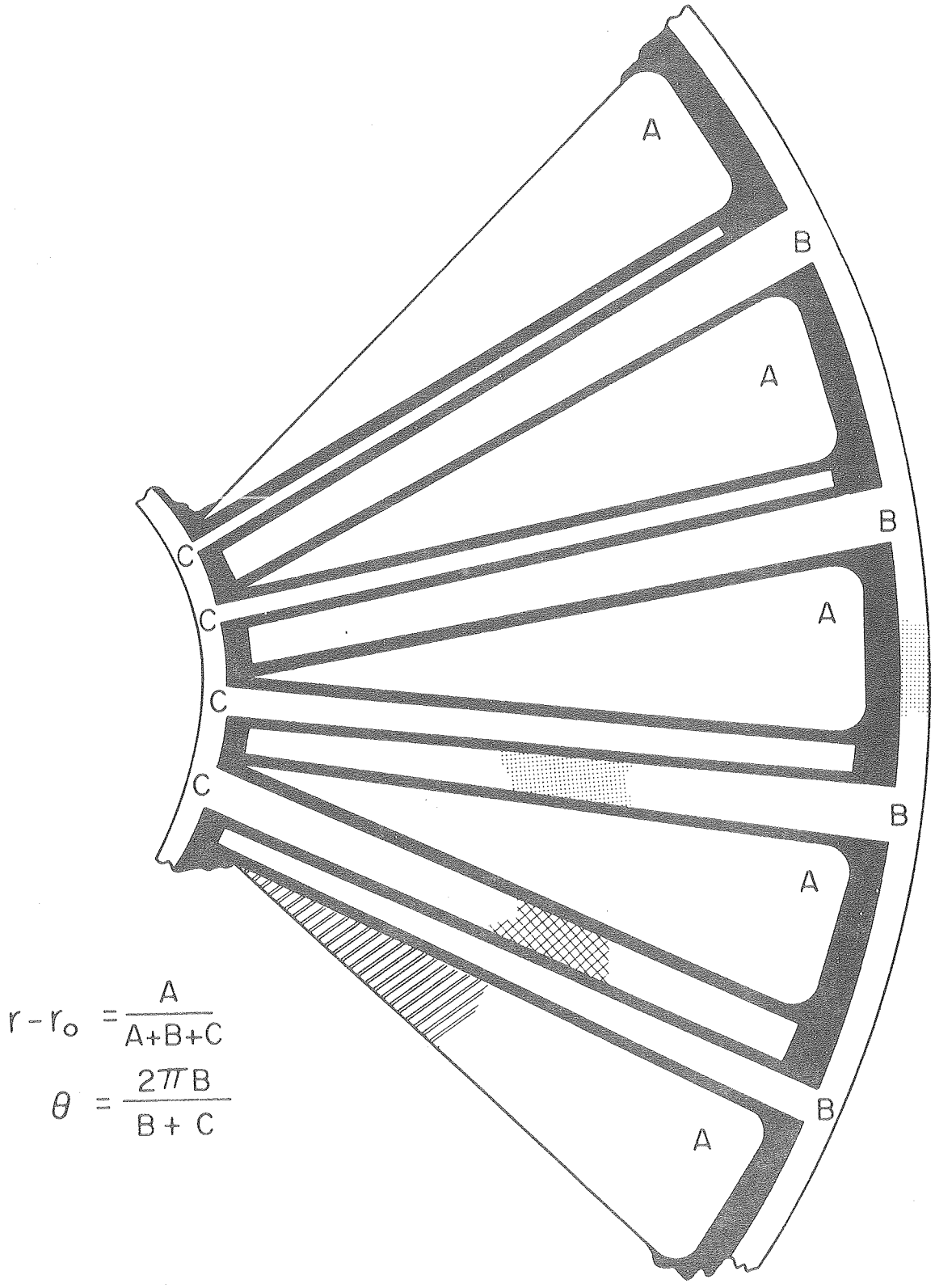

$$r - r_o = \frac{A}{A+B+C}$$

$$\theta = \frac{2\pi B}{B+C}$$

Figure 5: A polar coordinate anode. (Suggested by H. Gould.)

The readout need not be restricted to Cartesian coordinates. We have illustrated in Fig. 5 a novel design for a polar coordinate anode. This configuration provides an unobstructed central area, which facilitates experiments in which the center of the detector is located in the path of the light or particle beam.

V. FABRICATION AND TESTING

To verify the imaging characteristics set forth above, we have assembled two image systems, each using a tandem pair of microchannel plates, a wedge-and-strip-anode, three or four charge amplifiers, and a pair of analog ratio pulse position analyzers. The microchannel plates were Model 175 manufactured by ITT, which have a 40:1 length to diameter ratio, a bore 12 μm, and an overall circular field of view 25 mm in diameter.

Anodes were manufactured using techniques commonly employed in printed circuit fabrication. For our first anode, we adopted the pattern of Figure 2. The layout was created by applying strips of black tape to mylar film in the desired pattern of insulating gaps. A 1:24 photographic reduction was performed, and the resulting negative was used to contact print KPR sensitized epoxy fiberglass circuit board laminated with 7.5 μm of copper. The thinnest available metallization was used to prevent undercutting the narrowest conductors. The anode was etched and cleaned, and subsequently through-holes were drilled and wires soldered in place to electrically connect the individual elements of two of the conductors.

The finished anode is 25 mm square, and the conductor pattern has seventeen quartets with a period of 1.5 mm. The conducting elements are separated by insulating gaps measuring $\sim$ 30 μm. The capacitance between each conductor and the other three together measured 40pF.

The anode was initially mounted 6 mm behind the exit face of the rear MCP. The two MCP's were separated by a gap of 250 μm which was biased at 250-300V. Voltages of 750-800V were applied to the individual MCP's, resulting in overall mean gains of $0.6 - 3.5 \times 10^6$. At the lowest gains the pulse height distribution was flat with a Gaussian roll off. At gains above 1.5×10^6, the pulse height became Gaussian with 160 - 200% FWHM, indicating that the MCP's were saturated.

The signals from the four anode conductors were fed into FET-input charge sensitive amplifiers with gains of 10^{13} volts/coulomb and 1 μsec time constants. The shaped output pulses were directed to a pair of analog ratio circuits which used the logarithm-exponential method to determine the coordinates of each event. The output of these circuits drove an xy-display oscilloscope, which was photographed in 20-40 second exposures to accumulate an image.

To explore the imaging properties of the system, a resolution mask was placed in front of the first MCP, and a shadowgram was formed by illuminating the detector with diffuse HeI 584Å radiation emitted by a hollow cathode discharge tube.[9]

The initial images exhibited periodic geometric distortions of the nature of those described in Section II. From the amplitude of the periodic distortions ($\pm$ 0.5% of full scale) we inferred that the ratio of the charge footprint rms radius to the quartet period was approximately 0.5. To allow the electron cloud to expand further, and thus to increase this ratio, the anode-MCP gap was increased to 11 mm. No noticeable periodic distortions were present in these images. On the other hand, considerable overall distortion occurred which we attribute to stray electrostatic fields and protruding solder destroying the planar geometry of the electric field in the

post-acceleration gap. Nonetheless, this first anode exhibited excellent resolution: the smallest set of test bars, separated by 100 μm, were easily resolved at both low and moderate gains. We have estimated the resolution to be better than 50 μm at a mean gain of 3×10^6, giving 500 x 500 pixels over the 25 mm field of view. The dominant contribution to the random position error is amplifier noise, measured to be 1300 rms electrons.

The second anode was fabricated to test a new conductor geometry and etch mask production technique. The pattern chosen, shown diagrammatically in Fig. 4 eliminates the necessity for subplane connections, considerably simplifying fabrication and providing a planar electrostatic field. A 10:1 master layout was made with a computer controlled photographic plotter incorporating a numerically driven head. This technique permits a mask of essentially arbitrary dimensions and pattern density to be produced rapidly at very little cost. The pattern was then photographically reduced and used as a contact printing mask in the standard procedure employed to make the first anode. The finished anode, shown in Fig. 6, measures 35 x 35 mm. Each electrode has 33 individual elements, repeating with a period of 1 mm, gap widths between conductors of 50 μm, and a capacitance as defined above of 95 pf for two of the electrodes and 160 pf for the third electrode.

We emphasize the simplicity of this technique, which allowed an anode with suitable dimensions to be fabricated start to finish in a space of three weeks, for a cost of several hundred dollars. This system, using at most four amplifiers, is to be contrasted with the multiwire, multiamplifier readout system employed by other workers which require substantial investments of resources for fabrication, testing, and maintenance.

The second anode was installed in the small housing shown in Fig. 7, which included guard rings to establish a planar electric field in the anode

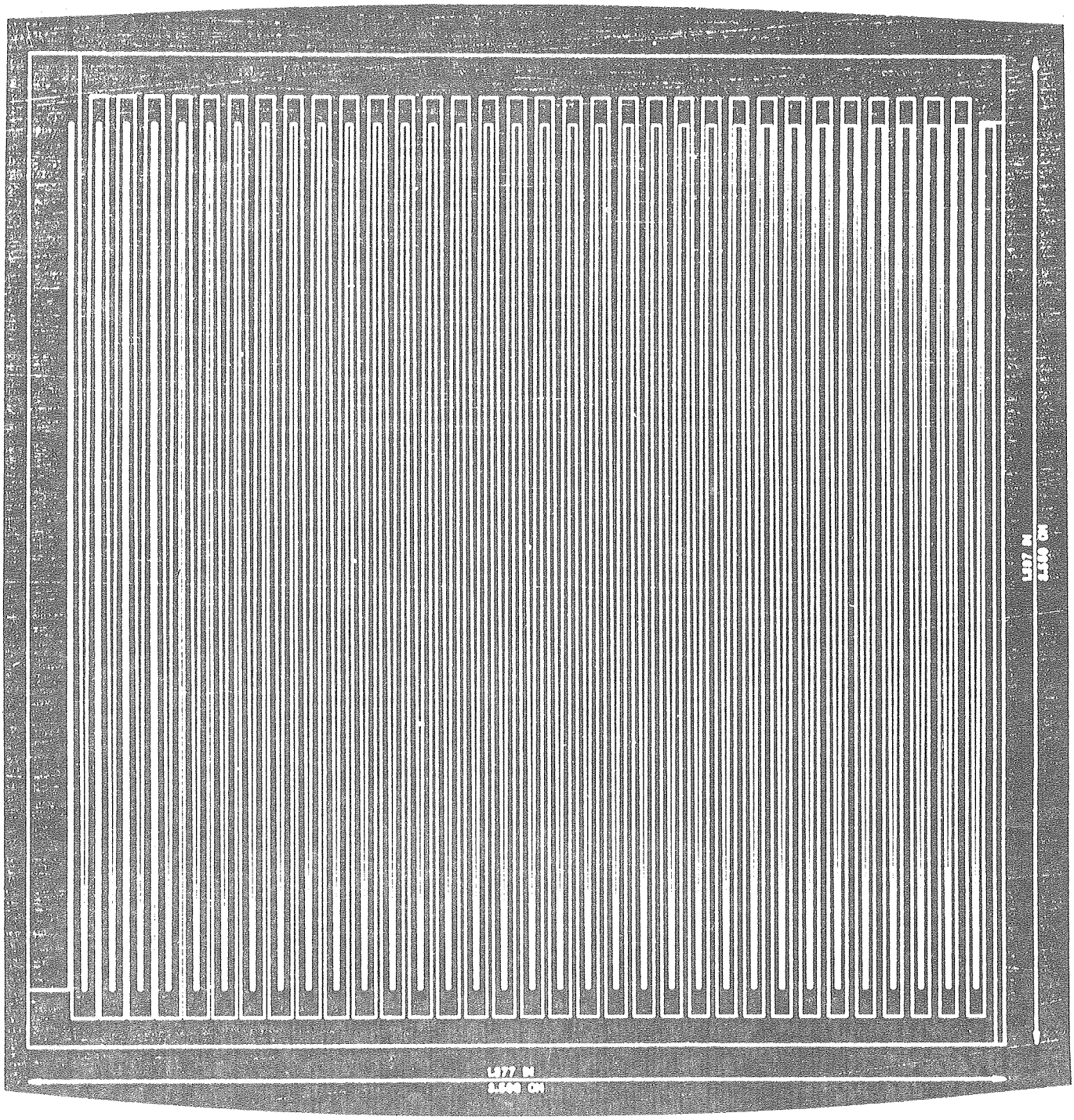

Figure 6: Photograph of an anode with the three conductor pattern of Figure 4. There are 33 electrode element groups repeating with a 1mm period. The anode was photo-etched on copper laminated onto epoxy fiberglass.

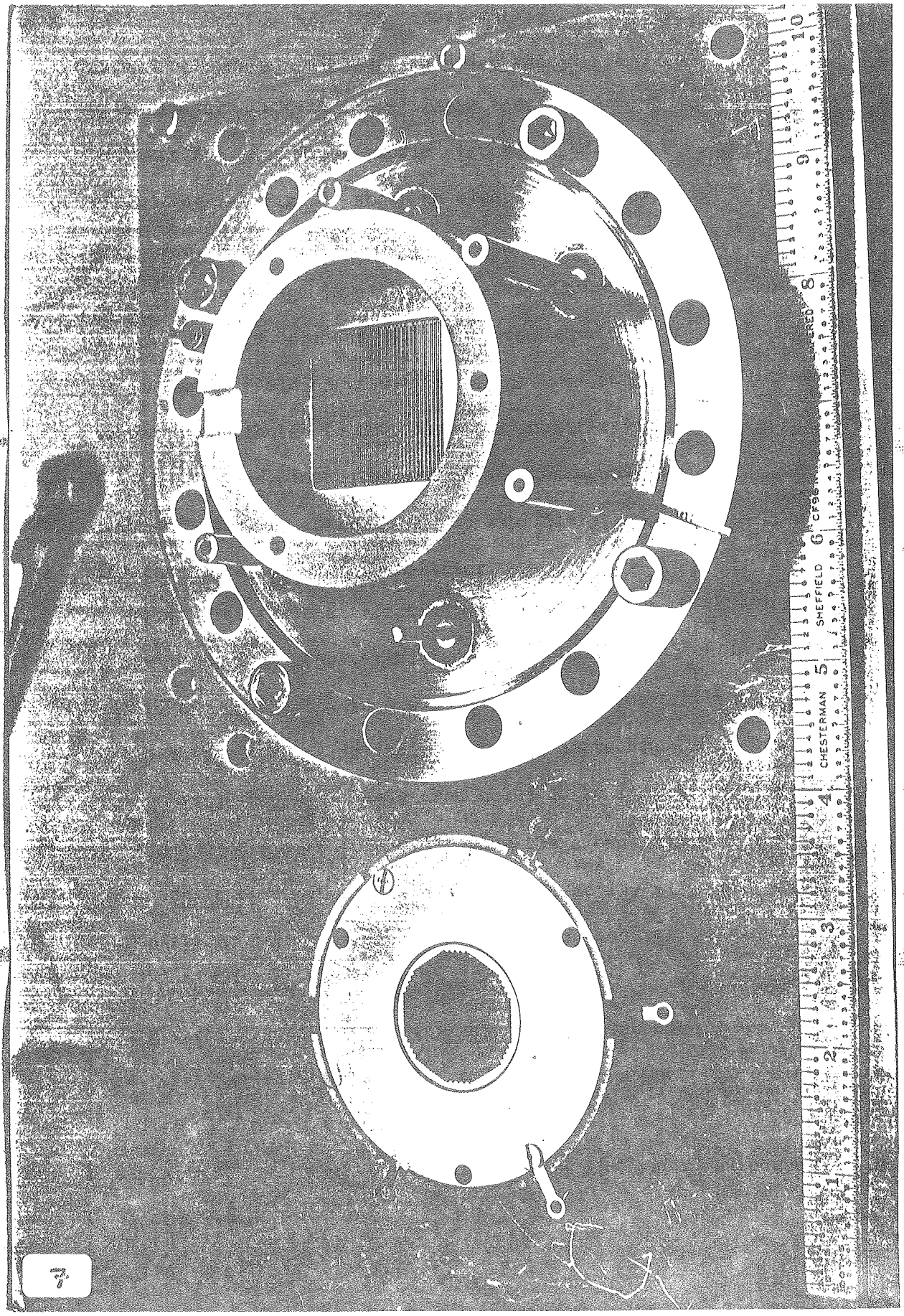

Figure 7

Figure 7: Detector for UV and EUV radiation comprising two MCP's and the anode shown in Figure 6. The vacuum flange incorporates high voltage and signal feed-through connectors.

gap. The gap was 12.5 mm. With a MCP gain of 3×10^6, and an anode gap potential of 300V, an image of the resolution test mask was obtained and is shown in Fig. 8. The periodic distortion was observed to be less than $\pm$ 0.05% of full scale. Fig. 9 shows an electronically expanded image of the smallest test bars, while Fig. 10, the one dimensional profile of a strip of the resolution mask image is plotted, clearly illustrating that a resolution of better than 100 μm has been obtained, yielding approximately 250 x 250 pixels over the 25 mm useful field of view. The slight reduction in resolution of the second anode is attributed to the increased amplifier voltage noise associated with the larger anode interelectrode capacitance, measured to be 1600 electrons rms for wedge and strip electrode amplifiers, and 2100 electrons rms for the zigzag electrode amplifier.

To investigate the effect of post acceleration on the image quality, the anode gap voltage was varied from 40 to 1600 volts, while the MCP gain was varied from 1.5×10^6 to 4.0×10^6. At the lowest MCP gains, since the space charge density in individual exit microchannels is small, we expect the space charge expansion of the electron cloud to be least[10]. At the same time, a large anode gap voltage will allow the cloud less time to expand. Thus we expect distortions to be most evident at low gains and high anode potentials. At a mean gain of 1.5×10^6, an anode gap potential of 1600 volts, the periodic distortion is approximately $\pm$ 0.3%., implying that the charge footprint rms radius is larger than 0.5 mm even under these conditions. For gains greater than 2×10^6 and an anode gap potential smaller than 1000 volts, the periodic distortion is less than $\pm$ 0.1%. The position resolution is not appreciably affected by the anode gap potential, as is expected.

Figure 8

Figure 8: Image taken using a Buckbee-Mears type JT4.2-1963 test target in contact with the detector, illuminated with diffuse 584 Å radiation. Exposure time = 10 sec., count rate = 5000 cps, image scale = 2.5mm/large division.

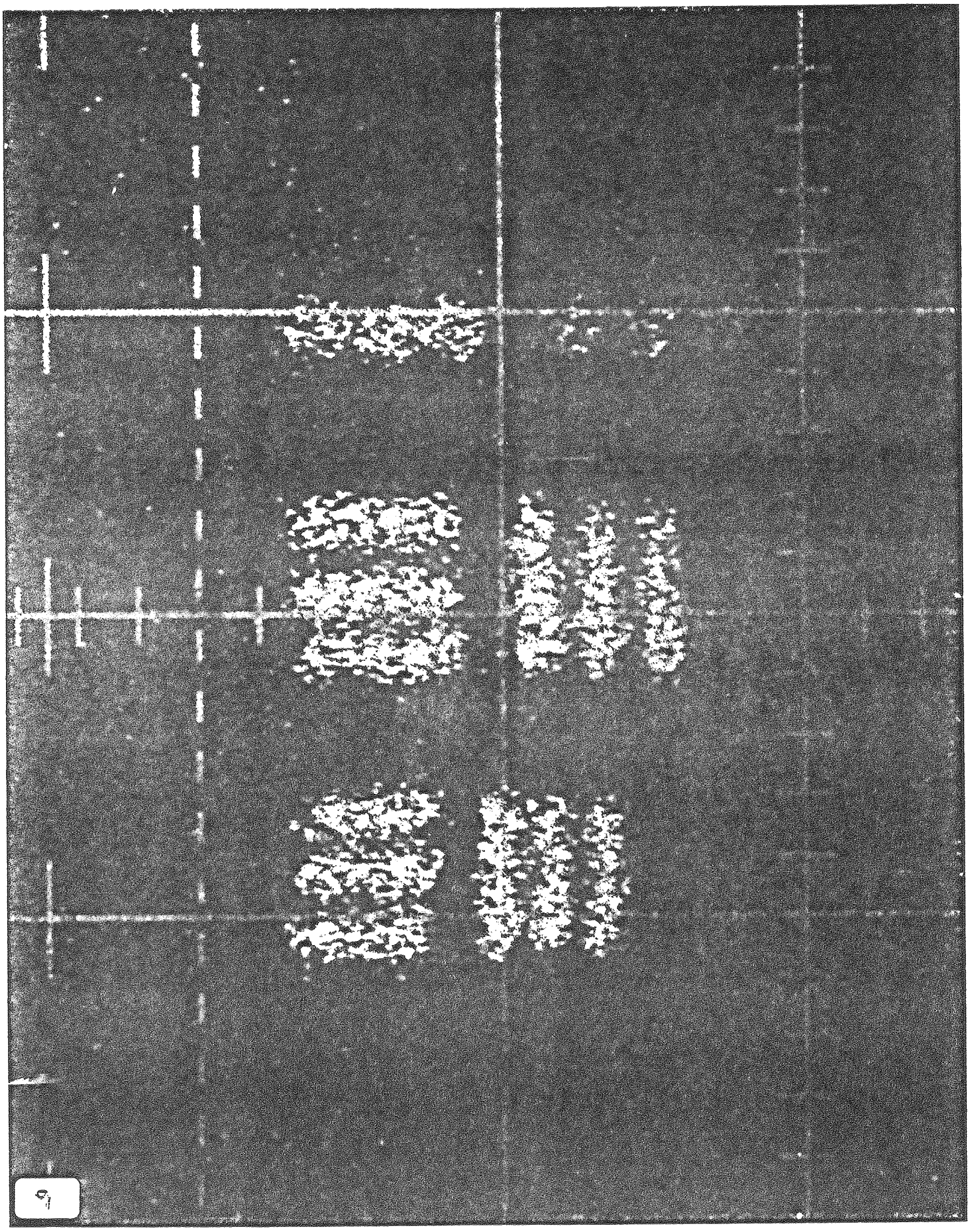

Figure 9

Figure 9: Image as in Figure 8, but with magnified display; the smallest image bars are 100μm wide.

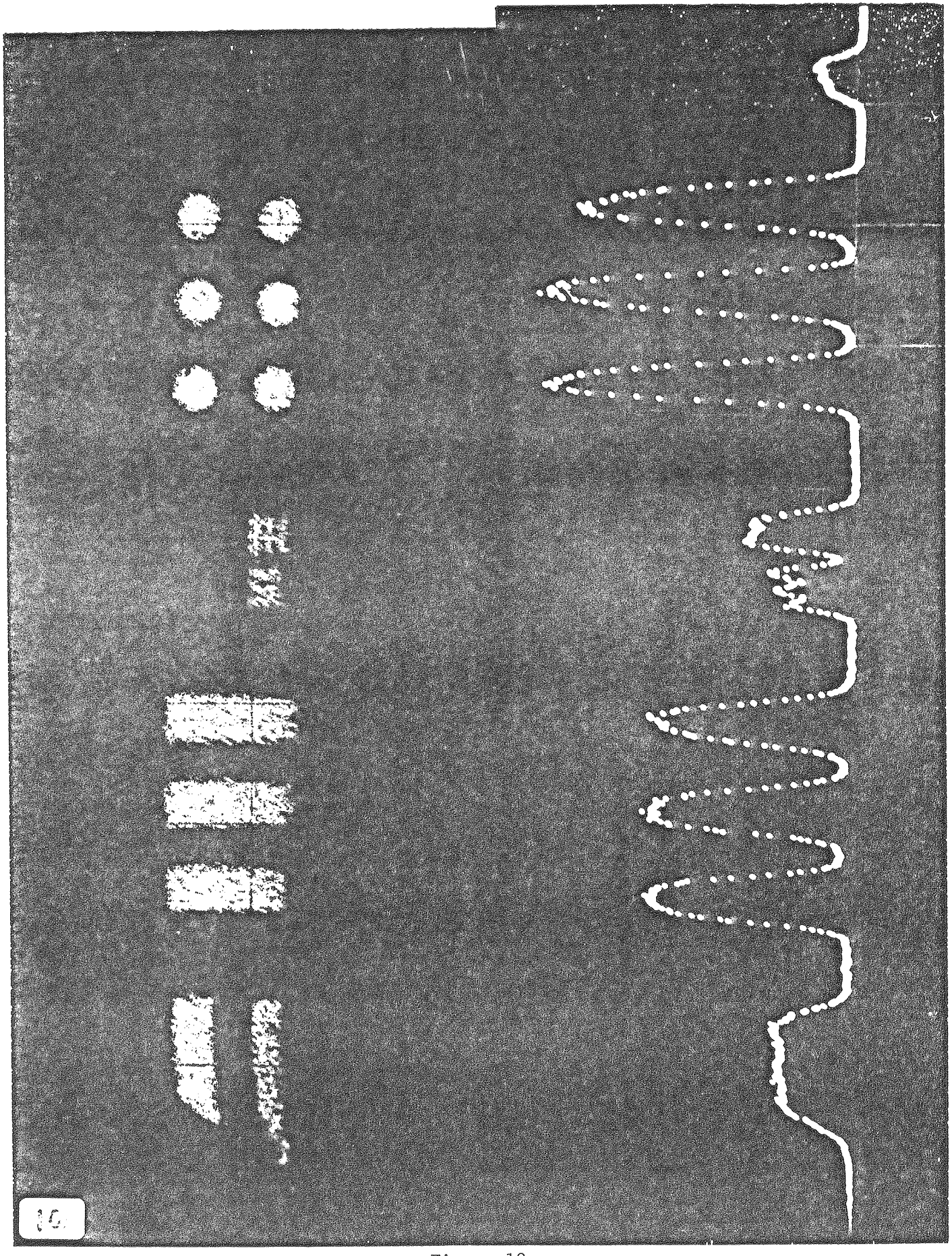

Figure 10

Figure 10: Histogram of a portion of image shown in Figure 8 showing the profile of the spatial density of the counts along the y axis. Image scale as in Figure 8.

In Fig. 11 the observed position blur, expressed as the FWHM of the point spread function, is plotted as a function of MCP gain, along with the predicted sources of blur. The points display measurements taken with capacitively induced pulses. The crossed bars illustrate results obtained with the MCP gain adjusted to allow the peak of the pulse height distribution to fall within narrow acceptance windows. The width of the bars represent the range of pulse heights accepted for each analysis. The individual contributions to the random position error, discussed above in section III, are represented by solid lines. Note that the amplifier noise contribution dominates in our present system. We point out that with a moderate increase in MCP gain (to $\sim 10^7$), and minor improvements in the ratio circuit electronics, resolution comparable to that of the High Resolution Imager (HRI)[11] on the Einstein Observatory would be obtained.

VI DISCUSSION

The theoretical and experimental findings presented here suggest that the wedge-and-strip anode can be applied to a variety of position-sensitive detector applications. First, in demountable mcp-based image systems sensing photons, ions, or electrons, this anode has the advantages over the resistive anode of potentially better spatial resolution, no dependence on the uniformity of a resistive film, and maximum possible charge collection speed. Second, it has a considerable advantage over quadrant anodes in being essentially distortionless, with uniform resolution over a large rectangular or circular field of view. Third, the fact that only three amplifiers and two ratio circuits are needed to locate events makes the wedge-and-strip system considerably simpler and less expensive than crossed-

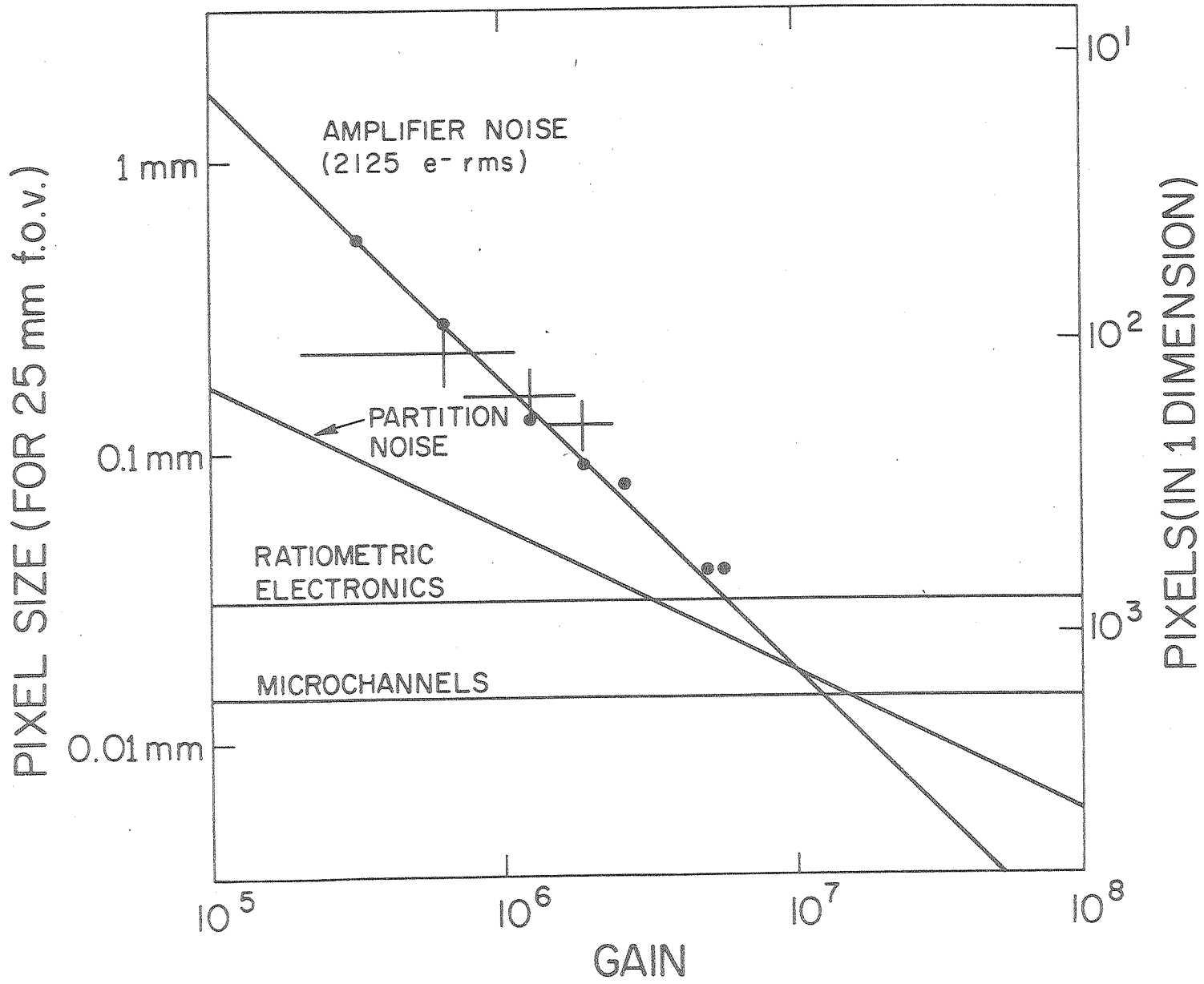
AMPLIFIER NOISE
(2125 e⁻ rms)
PARTITION
NOISE
RATIOMETRIC
ELECTRONICS
MICROCHANNELS
1 mm
0.1 mm
0.01 mm
PIXEL SIZE (FOR 25 mm f.o.v.)
10¹
10²
10³
PIXELS(IN 1 DIMENSION)
10⁵
10⁶
10⁷
10⁸
GAIN

Figure 11

Figure 11: RMS position error versus MCP gain. Solid lines show theoretical contributions from partition noise, amplifier noise, ratiometric electronics noise, and microchannel granularity. Dots indicate measurements taken using capacitively induced pulses, lines illustrate measured blur with MCP gain falling within narrow acceptance windows.

wire coincidence readout systems. A further bonus is that the wedge-and-strip electrodes are coplanar, which permits such anodes to be manufactured by electrochemical photographic etching (an inexpensive and reproducible process), giving the electrodes a rugged substrate support impractical with orthogonal wire gride anodes. Fourth, because the conductor pattern and substrate can easily be made using materials compatible with a high vacuum bakeout, we anticipate that a sealed position-sensitive microchannel photomultiplier tube for visible or ultraviolet work would be practical. Finally, the anode could in principle be adopted for use with sensors other than microchannel plates, such as planar gas proportional counters, multiwire gas counters, or focussed mesh dynode electron multipliers.

ACKNOWLEDGEMENTS

This work was supported by Cal Space grant CS 37-79. NASA contracts NAS-5-2445 and NAS-8-32577, and the U.S. Department of Energy under Contract number W-7405-ENG-48.

REFERENCES

1. M. Lampton and F. Paresce, Rev. Sci. Instrum. 45, 1098 (1974).
2. R. Allemand and G. Thomas, Nucl.Inst. Methods, 137, 141 (1976).
3. E. Mathieson, G. C. Smith and P. J. Gilvin, J. Phys. E 13, 792 (1980).
4. M. Lampton and R. F. Malina, Rev. Sci. Instrum. 47, 1360 (1976).
5. R. W. Wijnaendts van Resandt, H. C. den Harink, and J. Los, J. Phys. E 9, 503 (1976).
6. M. Lampton and C.W. Carlson, Rev. Sci. Instrum. 50 1093 (1979)
7. H. O. Anger, U. S. Patent 3.209,201 "Beam Position Identification Means" Sept. 28, 1965;
   H.O. Anger. Instrum. Soc. America Transactions 5, 311 (1966).
8. P. Jelinsky and D. C. Martin, in preparation (1980).
9. F. Paresce, S. Kumar, and C. S. Bowyer, Appl. Opt. 10 1904 (1971)
10. J. L. Wiza, Nucl. Inst. Methods, 162 587 (1979).
11. E. Kellogg, P. Henry, S. Murray, and L. Van Speybroeck, Rev. Sci. Instrum. 45, 282 (1976).